LAWRENCE
LIVERMORE
NATIONAL
LABORATORY

UCRL-JRNL-211387

# X-ray Scattering Techniques for Characterization of Nanosystems in Lifescience

C. K. Saw

April 14, 2005

Nanotechnologies for Life Sciences, Volume 3, Nanosystem Characterization Tools in the Life Sciences, Edited by Challa S. S. R. Kumar

X-Ray Scattering Techniques for Characterization of Nanosystems in Lifescience

*Cheng K. Saw Ph.D.*
*Materials Science & Technology division*
*Lawrence Livermore National Laboratory*
*Livermore, CA 94551*

## I. Introduction:

The intent of this chapter is to provide the basics of using x-ray diffraction techniques in order to obtain information on the structure and morphology of the nanosystems, and also to point out some of its strengths and weaknesses when compare to other characterization techniques. X-ray scattering examines over a wide range of density domains from a tenth to a thousandth angstrom. Essentially, this covers a whole range of condensed matter, including the structure and morphology of nanosystems, particularly useful for examining nanostructures in lifescience. This range of domain size requires both the wide-angle x-ray scattering (WAXS) and small-angle (SAXS) x-ray scattering techniques. Roughly WAXS covers from 2 nm down, and SAXS covers from .5 nm to 100 nm and possibly 1,000 nm for a finely tuned instrument. Brief theoretical description of both WAXS and SAXS will be given in this chapter. WAXS, by itself is a powerful technique in providing information on the crystallographic structure or lack of structure, atomic positions and sizes in a unit cell, to some extend, chemical compositions and as well as chemical stochiometry. Examples of such experiments will also be given. In order to be able to describe the technique of x-ray scattering, some historical and theoretical background will be given in the hope of making this subject interesting and simple.

Over the past 10 to 20 years, the major development in this scattering technique is in the instrumentation. Better and faster detectors are developed. Solid-state detectors and position sensitive detectors clearly play an important role in energy discrimination and high-speed data acquisition. The x-ray beams are conditioned with latest technology of using monochromators, mirrors and multi-layers and they can also be made to focus or collimate to the desired probe sizes without significant reduction in x-ray flux. The x-ray optics has been drastically improved. Improvements in the data quality have been demonstrated. The basic theory regarding x-ray diffraction and interactions of x-ray with matter developed in the early nineteen hundreds remains. With the coming of synchrotron radiation used for materials probe, a quantum leap is realized in all aspect of diffraction capabilities. Some of the examples will be pointed out in the later part of this chapter.

By and large, x-ray diffraction capability is a major component and necessary part in any modern characterization laboratory. In most cases, several diffraction instruments are needed for numerous reasons, for example, high through-put, different x-ray optics for high resolution requirement, different incident energy may be needed, different scan types and so on. Some of these will be more apparent in the later part of this chapter. In general, x-ray scattering technique is the quickest and cheapest method to obtain a whole lot of structural information. For example, identification of crystalline phases, phase impurities, additional disordered phases and the quality of the phases as well as lack of phases. It is also non-destructive and requires very

little, if not, no major sample preparation effort. In today's technological world, the structural information are required on very different sample types, for example, thin films, multilayers, very small amount of samples, specific crystalline orientations, residual stresses and so on. X-ray diffraction has also played an important part in protein crystallography where high quality data with enormous number reflections are needed for analysis to determine the structure of the protein. Clearly, so much sophisticated demands have been put on the technique the experimental setups have to be somewhat unique for each case of investigation. It is also the intent of this chapter to point out the experimental difficulties and ways to compensate and optimize the scattering properties, when carrying out these types of experiments on different nanosystems. These small and unique changes in the set-up will determine the quality of the data and thus, the success of the experiment.

Undoubtedly, x-ray scattering techniques also play a major role in obtaining information of both the structure and morphology of materials in the nanosystems in lifescience. Clearly, the understanding of structure and morphology of materials is the basic requirement for one to design and generate materials curtailing to the needs according to the desired functions. Other characterization techniques, well established over the years for materials science will also play major roles in the characterization of nanosystems for lifescience applications.

When higher resolution or sensitivity experiments are needed, they can be carried out using more sophisticated national facilities, like the synchrotron and the neutron sources at a number of major research facilities. In fact, the development of the synchrotron sources for characterization purposes represents a major advancement for x-ray scattering techniques. Experiments which are not possible or rather, very difficult to perform, using the in-house sources can now be easily performed on one of the beamline at the synchrotron source. It has greatly enhanced x-ray scattering capabilities. Most of these national facilities are opened to general users around the world. Synchrotron radiations are also x-rays. In this case, the x-rays are highly collimated, polarized, tunable and also has enormous brightness. Many new techniques, for example, absorption spectroscopy, anomalous scattering, elastic scattering and diffraction at different energies and high spatial resolution techniques (microprobes), just to name a few, are being developed. To enhance the atomic speciation, anomalous WAXS and SAXS have also been developed and often used in an advanced laboratory. This arises from the tenability of the x-ray to the desired energies close to the absorption edges to enhance the scattering power by taking advantage of the anomalous scattering factors. These techniques will be covered in subsequent chapters of this volume by other authors.

In general, nanostructures are crystalline structures with very small crystallite sizes in the nano-meter range. However, they can also be disordered in the angstrom domains by highly ordered in the nanometer range. If the sizes are small enough, the diffraction peaks are essentially very broad. As the size gets smaller, the material goes from a paracrystalline and eventually ends up to the amorphous state. The author will devote some time in describing the concept of small crystallite size, paracrystallinity and briefly touch on "structures" in an amorphous structure.

Nanostructures in the application of nanostructure technology, very often, are formed with some kind of coating around each particle to prevent agglomeration, or the fusing of the particles to form a bigger crystallite size. The characterization of this size domain is generally well suited

and carried out using the small angle x-ray scattering technique (SAXS). SAXS technique is also used to examine morphology and the molecular ordering in lifescience, particularly with proteins, micelles and lipids. Essentially, there are two major cases when using the SAXS technique, namely dilute and highly correlating systems. Dilute system refers to non-interacting nanostructure entities, which can be in examining proteins and micelles in solutions, for example. Highly correlating systems, for example, can be lipids and collagen where the overall molecules are highly ordered. In other situations, particularly polymer chains, mass fractal analysis is required. This will not be discussed here. Readers are encouraged to examine foundation books listed in the reference section. A number of fundamental x-ray diffraction books that I used to formulate this article are listed in the reference section [1-13].

This article is organized in the following sections while maintaining historical and developmental flow.



## II. Brief historical background and unique properties

In 1895, Wilhelm Konrad Röntgen, while experimenting with electric discharges in a tube noted that a barium platinocyanide treated paper lights up as a result of fluorescence induced by an unknown so-called x-rays. The x-ray originated from the tube and has great penetration power, which is found to be inversely proportional to the atomic number. The earliest application of x-ray was used as radiography in surgical operations, which clearly revolutionized the medical field. For this discovery, Röntgen won the Nobel Prize in 1901. Another prominent discovery was by C.G. Barkla, who noted that there is a homogeneous energy component in the emitted x-ray operating under certain conditions and is characteristic of the target elements. He also noted that there are 2 main groups of emission lines, known as K and L lines, which clearly play a

major role in Niels Bohr atomic model. For this he won the Nobel Prize of 1917. As the theory developed, x-ray was found to be electromagnetic radiation with the wavelength in the range of atomic spacing. Friedrich and Knipping first recorded the diffraction diagram of copper sulfate crystal. With this information Laue formulated the theory of diffraction, which won him the Nobel Prize in 1914.

It was W.L. Bragg who provided the explanation and correlation of the x-ray spots with the atomic spacing and suggested that the diffraction of x-rays are indeed caused by planes of atoms arranged in a lattice. Together with his son, W.H. Bragg, the first x-ray spectrometer was built and the quantitative diffracted intensity and angular positions were carefully recorded. As the result, the concept of diffraction was described and Bragg's law was introduced. These findings won them a Nobel Prize of 1915.

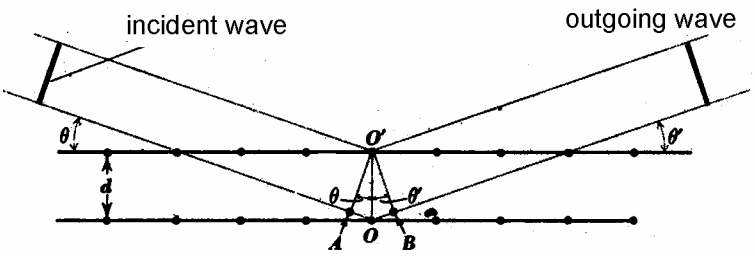


Figure 1: Diagram showing the constructive interference of the monochromatic x-ray.

This phenomenon is explained by supposing that the wave property of the x-rays are scattered individually by the atoms spherically, in the lattice as shown in Figure 1. The scattered waves are then interfered either constructively or destructively at some distance away in space. Therefore, it is a phase issue. In order for the waves to add up constructively, Bragg condition has to be satisfied. That is,

$$n\lambda = 2d\sin\theta \qquad (1)$$

where $n$ is the order of reflection, $\lambda$ is the incident wavelength, $\theta$ is the observed angle and $d$ is the inter-atomic spacings. The right hand side of the equation is essentially the difference in path lengths when the waves are scattered at positions O and O' as indicated in Figure 1. These d-spacings are generated by the atomic locations of positions in lattices. As a result, many crystal structures were found, lattice spacings were accurately measured and also, the characteristic x-rays from different elements were found and better defined. This is indeed a big advancement in materials science and fundamental atomic physics.

At times, energy is often used to describe the x-ray, instead of wavelength and is related by,

$$E(KeV) = h\nu = \frac{hc}{\lambda(A)} \qquad (2)$$

where $hc = 12.4$, $h$ is the Planck's constant and $c$ is the speed of light.

## III. Scattering of X-rays

In order to see how the scattering theory developed, it is important to start by describing the scattering of x-ray by a charge particle, say electron. This result can then be carried over to represent the scattering intensity of assembly of electrons, say in an atom, and then to a larger volume of mass. In the interaction of x-ray with matter, which is essentially surrounded by electrons, therefore x-ray scattering is accomplished by x-ray-electron interactions. Essentially, there are 2 major components of scattered x-rays, coherent and incoherent, assuming monochromatic incident x-ray beam. Coherent refers those scattered x-rays, which have the same wavelength (energy) as the incident x-rays. Incoherent refers to those x-rays, which change the wavelengths (energies), implying that the incident x-rays deposited part of their energy to the charge particle. The incoherent component (also refers to as inelastic) is a slowly varying function over the scattering angles. The coherent component, which will eventually interact via diffraction are the elastic component, and will be considered in this chapter.

Classically, the x-ray is described as a wave and is represented by the electric and magnetic field components. The wave is then incident on a charge particle electron, which is then modified, either coherent or incoherent, and then spherically scattered. The x-ray intensity is proportional to the square of amplitude. The intensity of the scattering of x-ray by a charged particle is given by the classic Thomson formula [14],

$$I_e = I_o \frac{e^4}{m^2 c^4 R^2} \left( \frac{1 + \cos^2 2\theta}{2} \right) \tag{3}$$

where $e$ is the electron charge, $m$ is the mass of the electron, $c$ is the velocity of light, $R$ is the distance between the observer or detector and the electron. The component in parenthesis is referred to as polarization factor. As Warren [10] pointed out, the component to the left is the scaling number in the order of $10^{-26}$ for 1 electron however, even in milligram amount of sample, there are $10^{20}$ electrons. The scattering by individual atom with atomic number Z and can be written by as the summation of individual electron scattering.

This is not totally correct, since the electrons are not located at a point. There is an electronic distribution function around an atom. Hence, the structure factor $f$ is introduced into the scattering equation. This factor is an integral of the electronic density distribution function generally derived by empirical means. Without going into details of the derivation, the structure factor is given by,

$$f = \frac{4\pi}{e} \int_0^\infty r^2 \rho(r) \frac{\sin kr}{kr} dr \tag{4}$$

where $k = \frac{4\pi \sin\theta}{\lambda}$, $\lambda$ is the x-ray wavelength and $\rho(r)$ is the electronic density distribution.

So, $f$ is proportion to atomic number Z at zero angle and diminishes as high angle. It should also

be noted that this equation of the structure factor is valid only if the distribution is truly spherical and the x-ray incident x-ray energy is not close to the absorption edge. Due to the anharmonicity of the electron distribution function and the wavelengths near the absorption edges, the structure factor is more complicated and has two additional modifying terms,

$$f = f_o + \Delta f' + i\Delta f'' \qquad (5)$$

where $f'$ and $f''$ are the real and imaginary component, often refers to as the anomalous dispersion. The derivation of these factors will not be discussed here. These values are also found tabulated in the *International Table of Crystallography* [15].

## IV. Crystallography

As the results of the development of x-ray diffraction and the complexity of the Bragg's planes, a method of defining the x-ray peak positions and intensities need to be developed. This is essentially accomplished by mathematical development through space groups. Again, the results of this work were accurately tabulated in four book series of "International Table for X-ray Crystallography" and are widely used as reference by scientists. More detailed descriptions of crystallography can be found in many fundamental x-ray diffraction books.

The crystallographic planes generated by lattices defined by the space groups are correlated to the x-ray scattering peaks. Hence, it is important to know where the atoms are located and what kind of planes do they generate, in order to calculated the peak positions. Crystallography describes the atomic arrangements in a lattice, which are defined by atomic translations and rotations forming some kind of periodic arrangements. The smallest unique atomic arrangement used to generate the crystal by rotations and translations is called the unit cell. The unit cell parameters are defined by three axes and three angles defined by the axes. There are seven forms of large subgroups of crystallographic systems and fourteen unique Bravais lattices for the atoms to arrange themselves. The seven systems are triclinic, monoclinic, orthorhombic, tetragonal, hexagonal and cubic. Essentially, they are defined by the relationship of the lattice parameters of three axes *a, b* and *c,* and 3 axial angles $\alpha$, $\beta$ and $\gamma$ define by the axes. Table I lists the crystal structures and the characteristic parameters of the axes and angle.

Table I: The crystal systems and their axes [16].

| System | Axes | Axial angle |
|---|---|---|
| Triclinic | $a \neq b \neq c$ | $\alpha \neq \beta \neq \gamma \neq 90°$ |
| Monoclinic | $a \neq b \neq c$ | $\alpha = \gamma = 90°$, $\beta = \neq 90°$ |
| Orthorhombic | $a \neq b \neq c$ | $\alpha = \beta = \gamma = 90°$ |
| Tetragonal | $a = b \neq c$ | $\alpha = \beta = \gamma = 90°$ |
| Hexagonal | $a = b \neq c$ | $\alpha = \beta = 90°$, $\gamma = 120°$ |
| Rhombohedral | $a = b = c$ | $\alpha = \beta = \gamma \neq 90°$ |

| | | |
|---|---|---|
| Cubic | a = b = c | $\alpha = \beta = \gamma = 90°$ |

With the atoms placed in the unit cell positions, the 14 unique systems can then be described. In the cubic system, there are three lattices, namely simple cubic, body-centered cubic and face-centered cubic. There are two tetragonal structures, simple tetragonal and body-centered tetragonal, four orthorhombic structures, simple, body-centered, end-centered and face-centered, and two monoclinic, simple and end-centered monoclinic. Additional atoms can be placed in each of the unit cells however these positions are simple equivalent positions.

These lattices generally have unique set of d-spacings, hence, in an x-ray diffraction experiments, these spacings are reflected in the intensity of the scattered x-ray at specific Bragg angles by these unique planes. Eventually, x-ray diffraction from crystal had progress level that a simpler way of identifying these planes had to be developed. This is accomplished by what is called Miller indices (*hkl*). The x-ray peak positions can be correlated to the type of lattices or space group.

## V. Scattering from a powder sample

The most common x-ray diffraction experiments are carried out on powder or bulk material with random crystalline orientation. Single crystal diffraction experiments are also being performed quite often, however, they have to be carried out using a four-circle goniometer. In situation when the unit cell is complex with a large number of atoms, single crystal experiment maybe the only way to extract the desired information on the structure. Single crystal experiments are generally far more complicated and difficult to perform without signification amount of experience. Also, when the samples are prepared, they are in the polycrystalline state. Therefore, the selection of single homogeneous crystal is often very tedious and difficult.

The total intensity from a powder pattern for a particular (*hkl*) at the angle 2θ is generally given by the scattering power [10],

$$P = I_o\left(\frac{e^4}{m^2c^4}\right)\frac{V\lambda^3 m|F_{hkl}|^2}{4v_a^2}\left(\frac{1+\cos^2 2\theta}{2\sin\theta}\right) \qquad (6)$$

where $I_o$ is the intensity of the primary beam, *e, m*, *c,* $\lambda$ and $\theta$ take their usual meaning, $V$ is the effective volume of the crystalline material in the powder sample, $m$ is the multiplicity for that reflection and $|F_{hkl}|^2$ is the structure factor square. The term with bracket on the right is known as the Lorentz polarization factor. For an actual experiment using a diffractometer, the scattering power is divided into per unit length of the diffraction circle.

In an actual experiment, Compton scattering needs to be subtracted, temperature factor needs to be added and the scattering power per unit detection length calculated. In most

cases, the slits, sample-detector distance is kept the same. Then, the scattering power is,

$$P = Km_{hkl}\left|F_{hkl}\right|^2 (LP)_{hkl} \tag{7}$$

$K$ is a constant with intensity proportional to the multiplicity $m_{hkl}$, structure factor square $\left|F_{hkl}\right|^2$ and Lorentz polarization factor $(LP)_{hkl}$. The structure factor is essentially,

$$F_{hkl} = \sum_n f_n e^{2\pi i(hx_n + hy_n + lz_n)} \tag{8}$$

where $f_n$ is the scattering factor which is directly dependent on the atomic number and

$e^{2\pi i(hx_n + hy_n + lz_n)}$ is the form factor which has the sinusoidal property and turns the intensity on or off. There are some exceptions to this rule and will be described below.

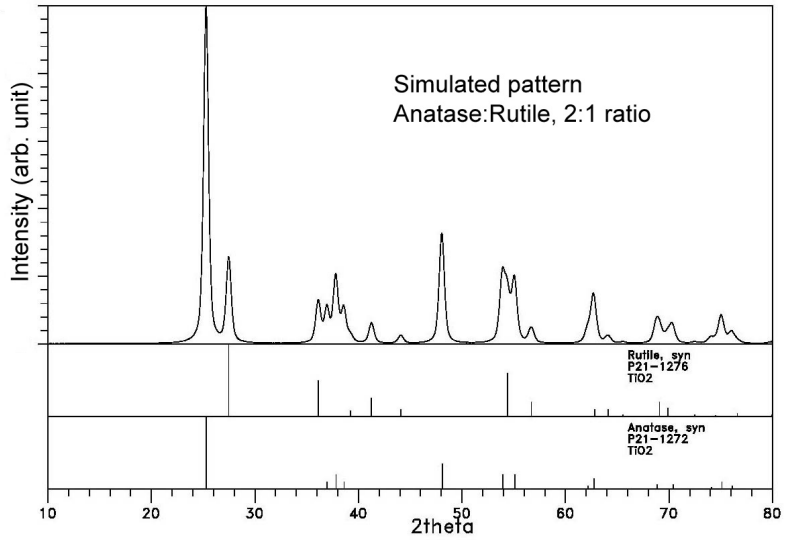


Figure 2: Simulated XRD pattern for 2 phases of titanium oxide.

A typical diffraction pattern is demonstrated in Figure 2 for a simulated pattern of two phases of titanium oxide, major phase is anatase and minor is rutile. Along with the plots are the reported peak intensities and positions from the ICDD database. Both phases have the tetragonal with different cell parameters. Thus, phases can be identified even though they came from the similar compound. Such results are commonly observed.

The structure factor as described in equation (8) is summed over all the atoms in the unit cell. For example, in the face-centered cubic (FCC) cell, for simplicity, there are 4 atoms located at (0,0,0), (0,½,½), (½,0,½) and (½,½,0). Equation (8) will become,

$$F_{hkl} = [1 + e^{\pi i(h+k)} + e^{\pi i(h+l)} + e^{\pi i(k+l)}] \quad (9)$$

and noting that $e^{\pi i m} = (-1)^m$, when *m* is an integer. Hence, it can be concluded that $F_{hkl} = 4$ if the indices *hkl* are all odds or evens and $F_{hkl} = 0$ when the indices are mixed. Now, lets turn our attention to body-centered cubic (BCC) structure and has 2 atoms (0,0,0) and (½,½,½) per unit cell. Equation (8) becomes,

$$F_{hkl} = [1 + e^{\pi i(h+k+l)}] \quad (10)$$

For $F_{hkl}$ to be non-zero, (*h*+*k*+*l*) must be even. Hence, in FCC, reflections occur when *hkl* are all even or all odd, but in BCC structure, *(h+k+l)* has to be even. For another FCC system, for example, rock salt structure of sodium chloride, having four Na atoms and four Cl atoms per unit cell, the summation in equation (8) will result in slightly different $F_{hkl}$. Again, the sample rule applied here that *hkl* have to be all evens or all odds. However, for the even case, $F_{hkl}$ will be four times the sum of their scattering factors, whereas for odd case, $F_{hkl}$ will be four times the difference of their scattering factors.

In the order-disordered structure of non-monatomic systems, it is possible to violate the above *hkl* requirements. This is because, even though the atomic positions are periodic, the atomic species may not. The scattering factors do not completely cancelled out resulting in the observation of non-allowed peaks. A good example is the well-known $Cu_3Au$ alloy [10]. Another system that needs to be considered is materials with antiphase domains where the atoms of different specie got interchanged resulting in super structures and x-ray diffraction peaks, not normally allowed.

## VI. Scattering by atomic aggregates

In practice, not all the matter in life has atoms arranged in nice lattices. The most interesting of these materials are those with complex atomic connectivity and having long atomic chains and do not have any kind of ordering in the unit cell range. Examples of such systems will be given in the small angle x-ray scattering section. The section will describe the component of amorphous and highly disordered scatterings. It is often very difficult to make a distinction between amorphous structure, similar to liquid or gas, and extremely small crystallite state, also sometime referred as a "para-crystalline" state. For nano-structures, it maybe important to determine whether the structure is amorphous or simply para-crystalline.

For time average scattering of non-interacting scattering like mono-atomic gases, the scattering is given by the Debye equation,

$$I_{eu} = \sum_m \sum_n f_m f_n \frac{\sin kr_{mn}}{kr_{mn}} \quad (11)$$

$f_m$, $f_n$ are the scattering factors, $r_{mn}$ are the inter-atomic distances. This equation can be represented in Figure 3 for $r_{mn}$ =1. This result clearly states that even for a non-interacting system, there is the ripple effect, which declines very rapidly going from low to high scattering angle. For polyatomic system, the result is still the same except that the ripples are much broader.

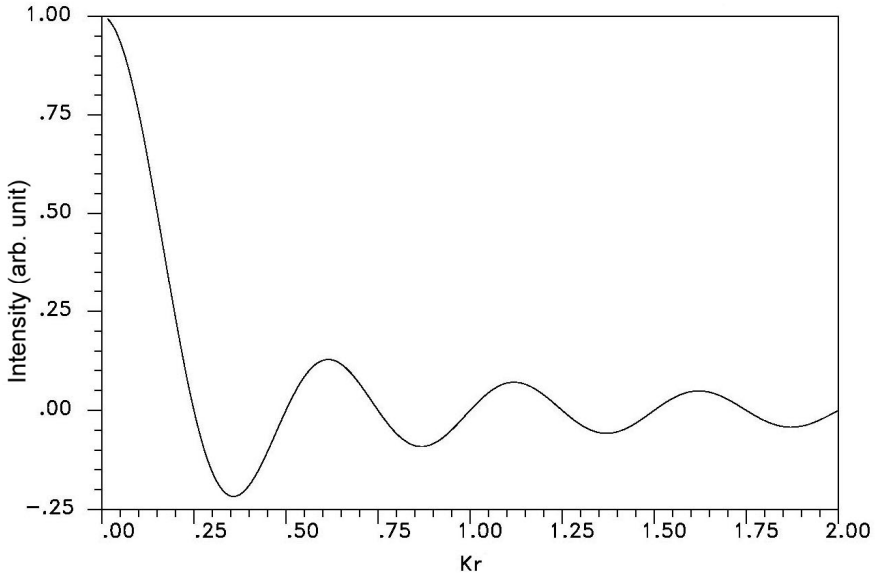


Figure 3: Intensity function of monatomic gas.

For a condensed system like liquid, the summation from the equation above can be simplified to

$$I_{eu} = Nf^2(1+\sum_m \frac{\sin kr_{mn}}{kr_{mn}}) \tag{12}$$

where the 1st term is the summation onto itself and the 2nd is the interacting term. This equation can then be converted to an integral,

$$I_{eu} = Nf^2\left[1+\int 4\pi\rho(r)\frac{\sin kr}{kr}dr\right] \tag{13}$$

Using algebraic manipulation and defining $\rho(r) = [\rho(r) - \rho_o] + \rho_o$, this equation becomes

$$k[i(k)] = 4\pi\int_0^\infty r[\rho(r) - \rho_o]\sin krdr \tag{14}$$

where $i(k) = \frac{I_{eu}/N - f^2}{f^2}$, for simplicity and by using the theorem of Fourier's conversion, we can write the radial distribution function as

$$4\pi r^2 \rho(r) = 4\pi r^2 \rho_o + \frac{2r}{\pi} \int_0^\infty k[i(k)] \sin krdk \qquad (15)$$

The above expression provided a mean of converting the intensity function, which is in *k* space to the radial distribution function in real space. In this formulation, the atoms are arranged in completely random fashion and amorphous. There are broad diffraction peaks, which belong to the amorphous structure. Unlike crystals, there is no crystallographic ordering. A number of papers have demonstrated on model calculations from ideal random atomic arrangements and determined the radial distribution functions. The density distribution function and be converted to the intensity or interference distribution function and can be compared to the experiments[17]. For binary systems with atoms of A and B species for example, the intensity function *i(k)* is actually a composite of the three partial functions $i_{A-A}(k), i_{A-B}(k)$ and $i_{B-B}(k)$. It is therefore, impossible to extract the each partial density distribution functions without further experiments. Because of differences in scattering factors for x-ray, neutrons and electrons, partial distribution functions can be extracted using a combination of the three experiments. Anomalous scattering experiments can and have also been performed to extract the partial distribution functions. By using the dense random packed models and comparing the calculated $i_{total}(k)$ with the experimental observations, the partial functions can be determined [18]. This is particularly useful in the understanding of atomic and chemical short-range order. Clearly, for ternary systems, the functions get very complex.

## VII. Crystallite size and paracrystallinity

Para-crystalline is used to describe small size ordering. Essentially, when the crystalline size is small enough, the resulting diffraction peaks will be broadened, however, the peak positions, if they can be de-convoluted will fall precisely at the crystalline positions. The extraction of the crystallite size from the peak widths can never be acute. Hence, in most cases crystallite size is generally an estimate. There are many factors that have impacts on the peak width, for example, lattice distortions possibly due to the thermal vibrations, micro-strains, nature of the paracrystallinity. In general, to improve the precision of extracting the crystallite size, the instrumentation broadening component can be subtracted out by performing the exact experiment of a highly order structure like powder silicon. The instrument factors are due to the misalignment, horizontal divergence (on a vertical Goniometer), energy spread of the incident beam, the interference of the $\alpha_1$ and $\alpha_2$ doublets, and also the absorption of the x-rays by the sample. It should be noted that the instrument broadening do not remain constant with all $2\theta$ angle but rather increases with increasing angle. For this discussion, we are only concern about determining the estimate crystallite size $D_{hkl}$ of the nanoparticles, it is generally given by the Scherrer equation,

$$D_{hkl} = \frac{K\lambda}{\beta \cos\theta_{hkl}} \qquad (16)$$

where $\beta$ is the peak broadening with the inherent instrument broadening subtracted out, $\theta_{hkl}$ is the Bragg angle measured at *hkl* reflection. K is normally taken to be 0.9 or unity, depending on the crystal shapes. For details on different values of *K*, refer to Klug and Alexander,Wang and Harrison. Figure 4 shows the plot of crystal size against x-ray peak broadening (FWHM- full width at half maximum) using equation (16) and assuming $2\theta_{hkl} = 20°$ indicating the sensitivity in the measurement of the small crystallite size and not large crystallite size. That is, a small change in FWHM translates to a large change in crystallite size in the small width region and small change in the crystallite size in the large width region. Very often, due to the uncertainty in the measurements, "apparent crystallite size" is used.

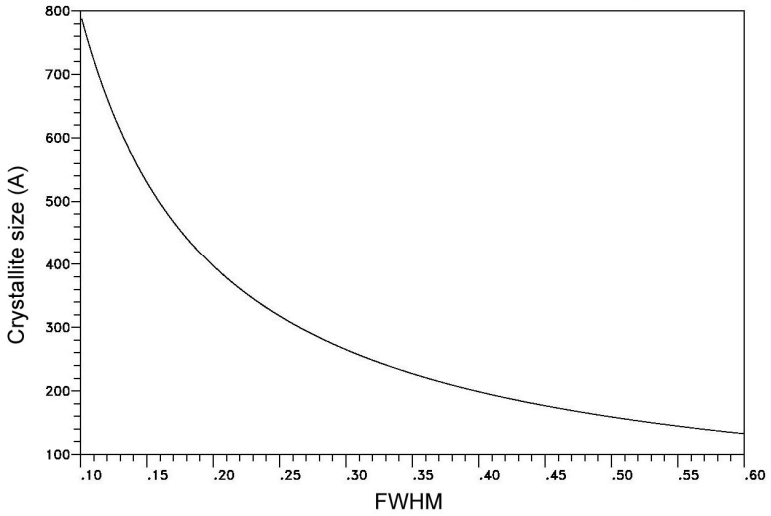


Figure 4: Comparison of the crystallite size versus FWHM.

As the crystallite size gets smaller, the peak broadens. Figures 5a and 5b compare the simulated diffraction spectra of crystalline cubic and hexagonal Co as a function of crystallite size, calculated using Jade software (MDI) for copper $K_\alpha$ radiation. Multiple peaks are observed in the hexagonal structure for crystallite size from 40 Å and above. Below 40 Å, the 3 distinct peaks between 40 and 50°(2θ) diminishes, hence it is not so clear whether the Co is either cubic or hexagonal phase. Moreover, without significant features, it can be concluded that the Co maybe essentially amorphous. Above 40Å, in this case should not be a problem in making the distinction.

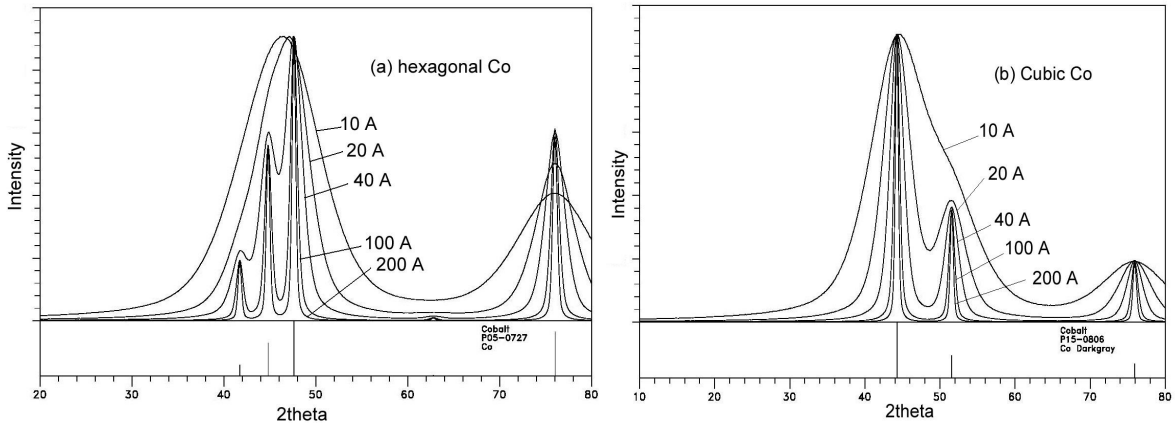


Figures 5a and 5b: Comparison of simulated crystalline Co of different crystallite sizes.

## VIII. Production of X-rays

At this point, it is important to understand the production and properties of the x-ray used in the probe. X-rays are generated when electrons emitted from a tungsten filament are accelerated with sufficiently high energy onto a specific target. Typically, x-ray tube voltages are set at 20 to 50 KeV. The interaction of the electrons and the electrons of the target materials resulted in a broad continuous x-ray spectrum. This radiation is often referred to as white radiation or the Bremsstrahlung (German for braking) radiation. This radiation is useful in the energy dispersive type of diffraction experiment or a Laue experiment for single crystals but is a nuisance in another when monochromatic radiation is needed. The energies and intensity of the Bremsstrahlung radiation is affected by changing the tube voltage.

With sufficiently high enough kinetic energy, the electrons can kick off bound (orbital) electrons from the target. Subsequently, the decay of higher bound state electrons to the lower bound state will result in the release of energy by emitting x-rays of characteristic energies or wavelengths, referred to as the K series with $K_{\alpha 1}$, $K_{\alpha 2}$, $K_{\beta 1}$ and $K_{\beta 2}$ radiations. The population of the $\alpha$ series is much stronger that the $\beta$ series. In general, most of the diffraction experiments are carried out using the $K_{\alpha}$ radiation and $K_{\beta}$ radiation is masked off by a number of techniques.

It is known that less than 1 % of the energy that is incident onto the target is converted to x-rays. Hence, this is a very inefficient method of generating x-rays. Most of the energy is dissipated as heat at the target. This heat energy needs to be removed immediately otherwise the targets can be melted away. In general, the targets are designed to be on top of a high thermal conducting heat sinker, which is also under constant cooling. Because of this heating issue, there is a limiting power that the x-ray generator can operate. This clearly depends on the tube design to achieve optimum cooling of the targets. Another target design, which allows for higher power setting is the rotating anode x-ray generators. The target element is deposited on a high thermal conducting rotating drum (usually made out copper), which is constantly being cooled. The drum rotates at a very high speed, thus making the target position where the electrons hit constantly

changing. This design elevates the heat dissipation problem and therefore, the higher power setting can be achieved, resulting in higher x-ray flux. Unfortunately, maintaining the vacuum condition via a rotating shaft is a challenge.

## IX. Absorption of X-rays

It is important to understand the absorption behavior of x-ray through opaque materials. In general, x-rays are absorbed whenever they pass through matter. The equation governing this rule is simply,

$$I = I_o e^{-\mu\tau} \tag{17}$$

where $I_o$ is the incident intensity, $I$ is the transmitted intensity, $\mu$ is the linear absorption coefficient ($cm^{-1}$) and $\tau$ is the thickness (cm) of the absorber. This is assuming that the x-ray energy is far away from the absorption edge. For convenient, the mass absorption coefficients, $\mu/\rho$ ($cm^2/g$) are used and tabulated [15].

$$I = I_o e^{-\left(\frac{\mu}{\rho}\right)\rho\tau} \tag{18}$$

Hence, the mass absorption coefficient is independent of density and the overall absorption coefficient will just be the summation of the coefficients weighted accordingly to the composition.

For x-ray energies close to the absorption edges, the coefficient of absorption changes abruptly. This is directly related to the work function required to knock off electrons from their original shells. The absorption coefficient can also be empirically calculated [15].

## X. Instrumentation: WAXS

The crystallographic structural information on nanoparticles has to be gotten using conventional x-ray diffraction techniques. In general, the most common diffraction experiments are carried out on bulk and powder samples. Again, in general most materials are polycrystalline. At times, single crystal experiments are very useful for obtaining detailed structural information, small lattice anisotropy and complex unit cell or cell with a large number of atoms. Single crystal experiments have to be carried out on a four-circle goniometer and will not be described here. Also, at times when special scans are needed, for example, for measurement of residual stress, pole figures, rocking curves and so on, four circle x-ray goniometer is needed.

The most common and widely used x-ray powder diffraction technique is the Bragg-Brentano method. It is self-focusing and optimize for intensity and resolution using the conventional

in-house x-ray sources. The x-ray optics is shown in Figure 6. This type of diffractometers is essentially very versatile. The distance from the source F to the sample and the sample to the receiving slit is always kept equal and constant at all scattering angle Parallel vertical slits P and RP are added to improve the scattering signal. D is the defining slit and R is the receiving slit. Because of the focusing requirement, alignment of the sample is critical for accurate peak position measurements. To help in the alignment and calibration, a known standard, for example, a well-characterized silicon powder standard from NIST is used.

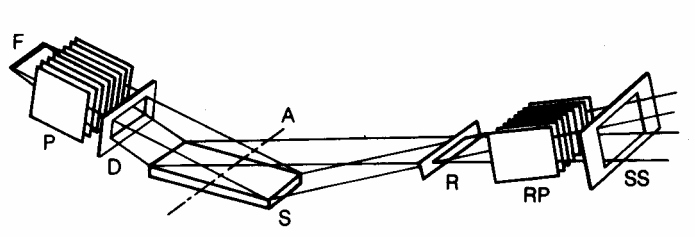


Figure 6: Para-focusing Bragg-Brentano geometry

Traditionally, the x-rays are detected using high sensitivity film. In some cases, they are continuing being used. The films are then processed and read by a digitizer, which is essentially a measurement of transmitted light over the spatial positions on the films. X-ray films are also used when examining two dimensional scattering. Because of the difficulty in processing the film, the modern version, image plate has been invented. In this case, an image reader is needed.

For pulse counting technique, gas ionization counter is used. The gas ionization counter, also known as Geiger-Müller counter, essentially consists of exposing a gas filled region, normally noble gas like argon, krypton or xenon, mixed with a small amount of quenching gas, held at high potential, to the x-ray. Normally, this region is protected by a transparent x-ray window. When the x-ray enters the compartment, it ionizes the gas, producing electrons. These electrons accelerated to the anode, thus creating a current pulse. The quantum efficiency of this detector greatly depends on the design and the type of gas it uses. The energy resolution is poor and the detector can be saturated without going to very high count rates.

A more convenient scintillation has also being development. This type of detector depends greatly on the fluorescence of certain crystals, for example, sodium iodide or cesium iodide crystal doped with thallium. Other crystals are also used. These crystals emit light when exposed to x-rays. The light is then converted to electron pulse via a set of multiplier plates which can then be counted by the electronics. In this case, the dead time is much shorter and counting for higher count rate can be achieved.

The energy resolution for the above two counts are not optimal for normal diffraction technique. The $K_\beta$ radiation and other background radiations, for example, contamination from the x-ray tube, need to be discriminated. Traditionally, foil filters are used. The selection of the foils is based on the absorption edges for example, when using copper $K_\alpha$ radiation, a nickel filter foil of

0.0158 mm is needed which will absorbed 98.4 % of the $K_\beta$ radiation [4].

Another way of removing the background radiation is the commonly use analyzing crystal (also called diffracted beam monochromator) placed right in front of the detector which can either be the gas proportional counter or the scintillation counter, after the receiving slit. The choice of the crystal is based on the crystal mosaic, for energy selectivity and the efficiency. The most widely use energy discriminator is usually graphite for efficiency without significantly scarifying x-ray intensity. For experiment with more stringent energy discrimination, LiH monochromator is used. In most cases, the analyzing crystal does not have sufficient resolution to remove the $K_{\alpha 2}$ radiation

Another way of improve the scattering signal is the used of the solid-state detector (SSD). Normally, the detector consists of Si(Li) (silicon-lithium drifted) or Ge(Li) (germanium-lithium drifted) held at liquid nitrogen temperature. When an x-ray impinges on the detector, an electron-hole pair is created and the number of electron-hole pairs is proportional to the energy. Hence, in this case, the energy resolution is roughly at about 130 eV. $K_\beta$ radiation can be eliminated as well as other background radiations and fluorescence from the sample.

Since the solid-state detector has such high energy resolution, energy dispersive diffraction technique is invented. Essentially, it takes advantage of the full broad energy spectrum of x-rays coming out from the tube because of the Bremsstrahlung radiation and by having the detector at specific angle, a full range of Bragg scattering can be gotten from the energy dispersion. The advantage here is that there is no moving part when conducting the experiment. It made use of the full range of x-ray and counting statistics can be greatly improved. The drawbacks are that Bragg peak width is significantly broader that the conventional scanning technique. The detector is big and clumsy, and has to be constantly liquid nitrogen cooled. However, newer version of SSD known as Peltier detector is electrically cooled. This is also rather heavy and clumsy as well.

A normal mono-energetic experiment makes use of the strong $K_\alpha$ radiations, which consists of $K_{\alpha 1}$ (8.04778 KeV) and $K_{\alpha 2}$ (8.02783 KeV) energies [19]. For cooper $K_\alpha$ radiation, $K_{\alpha 2}$ intensity is about half of $K_{\alpha 1}$. $K_{\alpha 2}$ radiation is essentially unwanted component of the incident beam. The difference in energies is about 20 eV. However, if a more stringent monochromator is used, the intensity will be drastically reduced. Most powder diffraction experiments simply ignore it. However, when one examines nanostructures where the crystallite size is very small, the presence of $K_{\alpha 2}$ will not be a factor. On the other hand, if one chose to use higher energetic radiation, like molybdenum, the difference is about 105 eV. Normally, the best solid state detector has a resolution of 130-150 eV.

Unfortunately, this setup is not favorable for samples with elements excitable by the incident x-ray with energy 8.04 KeV for copper $K_\alpha$ radiation, for example magnetic nanoparticles Fe and Co containing sample. In these situations, some form of tighter discrimination is needed to extract the coherently scattered x-rays and not the fluorescence from the sample, which is essentially noise for the diffraction experiment. A way to get around this problem is by changing the probe radiation to that of $CoK_\alpha$ for cobalt containing sample and $FeK_\alpha$ for iron containing samples. In this way the x-ray probe energies will not be sufficient to cause the fluorescence. By

changing incident x-ray energies, one has to be aware that the penetration depth is decreased and the energy discrimination needs to be readjusted. Another way to carry out diffraction experiments on highly fluorescence samples is to ensure that the incident energies are sufficiently far away from the fluorescence from the samples, for example, using $MoK_\alpha$ radiation on iron and cobalt containing samples. In this way, the diffracted beam crystal can easily be filtered out the fluorescent signals.

## XI. Small Angle X-ray Scattering

The regime covered by small angle x-ray scattering technique, typically covers the range from 0.5 to 100 nm and according to Bragg's equation, this turns out to be only a few degrees in $2\theta$. This regime also turns out to be a very useful range for the examination of many types of nanostructures. In general, for the application of nanostructures, it is customary to have a layer of polymeric coated on each particle. Information on size, shapes, inter-particle correlations and density fluctuations of nanostructure are of importance and can be obtained using this technique. In lifescience, for example, biological cells and cell tissues, proteins and protein folding, colloids, micelles, bacteria and viruses can also be investigated using SAXS. This technique has also been widely used in examining tumors and cancerous cells, and distinctions in the diffraction patterns between healthy and cancerous cells have been shown. It is the information on the macro-scale, the connectivity and arrangement of the local domains, that is critical in the understanding of the behavior of these systems. For example, SAXS has been used to examine healthy and cancerous human breast tissues and it is determined that the collagens structure are very different [20]. It has also been widely used to examine tumors and cancerous cells [21], and again, distinctions have been drawn between healthy and cancerous cells. Further research is continuing to understand the cause of cancer by many groups. Even so, by combining SAXS and WAXS characterization techniques, experiments can be carried out on well chosen cell tissue samples that will provide information for the understanding of disease processes evolution. This represents a new form of diagnostic capability for health sciences.

Information on the nanostructure, size, shapes, inter-particle correlations, density fluctuations are of importance and can be obtained. In lifescience, for example, biological cells and cell tissues, proteins and protein folding, colloids, micelles, bacteria, viruses and other lifescience systems can also be investigated using SAXS for ordering in the macro-scale. Most of these systems are highly disordered at the local level (angstroms) at times they are even semi-crystalline. Clearly, these systems are very complex and in most cases consist of interpenetrating components of different make-up of molecules. These molecules which can also be of odd shapes essentially hinder the formation of unit cell arrangements. Again, the macro crystalline arrangements that is critical in the generation of the properties.

Another example of using x-ray scattering experiments in lifescience is the understanding of

structure and morphology of bone. Bones are made up of fibrillar collagens with nano-particles of crystalline hydroxyapatite distributed in the macro structure. It is this macro arrangement of the collagen and the crystalline component that provides the optimal compression strength for the load bearing of the anatomy [22]. It is believed that there is a network of collagen fibers deposited and grown within and between the collagen fibrils [23]. The SAXS experiment can provide information on the macro domains. The area in lifescience that SAXS will play an important role is in the understanding of the cell membrane. Information on the structure of the lipid moieties in cell membrane essentially defines the functionality of the membrane [24]. Even though, lipids are considered to have the major bilayer structures, monolayer structures do exist. Of particular interest is the understanding of the lipid behavior in solvent, which again can be carried out using SAXS. Depending on the acquisition time, in-situ experiments as a function of temperature or time decay can also be carried out.

For nanostructures in biological materials SAXS analysis is used to extract information relating to the macro-lattice on highly correlating domains, which often can be periodic. Typical example for this is the tendons. Many biological systems also possess periodic structures for example, animal tail tendons and myelin membranes in the nerve. In polymers, the scattering signal arises from the stacking of lamellar crystals and block copolymers having segregating density domains.

For laboratory prepared nanoparticles (or crystals) for example, cobalt [25] when coated with organic layers self-assembled into superstructures. The structure and dimension of these superstructures are also examined using both the WAXS and SAXS, thus, providing a full description on the overall structure. Superstructure of biomaterials like colloidal particles of glycolipids has also been examined using SAXS. The technique was able to provide information on the structure of the dispersed particles [26].

The analysis of SAXS data essentially can be divided into three groups, namely dilute systems, highly correlating systems and fractals. In the dilute systems when the structures are non-interacting, information on the shape, size and mass of the molecules can be obtained. For highly correlating system, the basic formulation follows the Bragg's law. The fractal component is generally useful for polymers and polymer chains and will not be discussed here. The readers are encouraged to refer to other sources [7, 12].

## a. Dilute systems

The scattering for dilute systems assumes that the scattering from each particulate is independent of each other. Hence, it is critical for the sample to have appropriate thickness so that no multiple scattering can occurred. The x-ray interacts with the electrons fluctuations surrounding the particulates and the total intensity is merely the sum of all the individual scattering components. Therefore, information on sizes, shapes and mass can be obtained. The generalized scattering function is essentially given as,

$$I(k) = (\rho_o v)^2 F^2(k) \qquad (19)$$

where $\rho_o$ is the density difference over total volume $v$ and $F(k)$ is just the structure factor. The form factor is simply represented by

$$F(k) = \int \rho(r) e^{ikr} dr \tag{20}$$

where the integral is over the electron density over each particulate and the exponential component is the form factor. By expanding the form factor and dropping out the higher order terms, Guinier shows that the intensity function is

$$I(k) = \rho_o^2 v^2 \exp(-\frac{1}{3} k^2 R_g^2) \tag{21}$$

or

$$I(k) = I(0) \exp(-\frac{1}{3} k^2 R_g^2) \tag{22}$$

where *I(0)* is the scattering at zero angle. Essentially, this function is Gaussian over. Very often, $\log_e I(k)$ is plotted against $k^2$ and the radius of gyration $R_g$ can be extracted from the slope of the resulting linear curve. The shape information is obtained from $R_g$ and $R_g$ for many different forms of particulate has been calculated and will not be discussed here. Actually, $R_g$ is defined as

$$R_g^2 = \frac{\int_0^\infty \rho(r) r^2 dr}{\int_0^\infty \rho(r) r dr} \tag{23}$$

and describe as the root-mean-square distance of all points in the particle from the center of mass weighted accordingly. The size of the particle is conveniently expressed by $R_g$ and assuming the shape is known, the radius of gyration can be extracted accurately. The radius of gyration for some common shapes has been tabulated in many review articles. By knowing or assuming the shape of the particle examined, the dimension of the particle can be gotten by solving for the radius of gyration. The extrapolation of the Guinier plot to scattering at zero angle results in $\rho_o^2 v^2$, which provide information on the particle molecular weight and volume. However, in this case accurate intensity of the main beam is needed.

For homogenous particles with distinct boundaries between the particles and the matrix, which can be a solution or another media with different density, for example in polymers with crystalline and amorphous components, Porod indicated that the scattering $I(k)$ should decrease as $k^{-4}$ for large *k* and the proportionality constant is related is related to the total area S occupied by the boundaries and is expressed as,

$$I(k) = \frac{2\pi\rho_0^2 S}{k^4} = \frac{P}{k^4} \tag{24}$$

By plotting log ($I(k)$) versus log ($k$) and extrapolating to $k=0$, the $P$ (Porod constant) can be extracted. When this parameter is divided by the "invariant", which is the scattering intensity for the total volume, the surface area to volume ratio can be gotten. When this parameter is divided by the density, the total surface area (m/g) resulted. The information is particularly useful, especially in the area of catalysis when the amount of surface area controls the property of the material.

## b: Highly correlating systems

In most cases in lifescience, most of the systems are highly correlated or rather densely pack with significant density fluctuation and also highly oriented. For example, the collagens are very well packed in a fibrillar fashion and the diffraction pattern shows many orders of reflections. The peaks are also very sharp with dimension of 67 nm for native rat tendon [26]. Obviously, for the densely pack systems, the scattering theory is governed by Bragg's law.

Collagens are common occurrences in lifescience. It is a major constituent in tendon, bone, skin, cornea, cartilage and other parts which require strength and flexibility. Clearly, the packing and the deformation of the collagens will reveal the state of the matter, when comparing to a healthy tissue. The arrangement of collagen is believed to be liquid-crystalline like as well as large scale triple helices arrangements for roughly 300 nm [27, 28]. The changing of the packing indicates some kind of mineralization which is preventing proper function of the component. It is indeed a mystery that collagen which is abundance in our anatomy has so many functions. It is the arrangement in the macro-scale which changes its properties [29].

As described earlier [24], examination of protein bi-layers is of great importance in the biological science. Essentially, these are highly correlated systems. Clearly, the structure and the makeup of these bi-layers constitute the working of the membranes, peptides and etc. There are enormous numbers of biological systems that can utilized both SAXS and WAXS for the understanding the behaviors in lifescience. Biological systems are normally very complex.

# XII. SAXS Instrumentation

SAXS experiment, in principle has a very simple geometry, as shown in Figure 7, however improperly arranged and aligned components will result all kinds of problems, for example parasitic scattering, calibrations, peak profiles and background noise. The quality of the instrument greatly depends on the level of noise because the diffuse scattering intensity for most samples can be very weak for different reasons. A very well defined x-ray beam is needed for this application.

There are numerous SAXS instrumentations available commercially. Essentially, they are divided to two types of configuration, pin-hole and the line source technique. They each have their strengths and weaknesses. The pin-hole technique will be useful for examining anisotropic materials, for example, fibers, films and any sample with orientations. However, there is an inherent lost in intensity, resulting in long data acquisition time. A 2-dimensional detector system is required, for example conventional high sensitive x-ray film, image plate, 2D proportional gas detector and even the CCD (charge coupled device) detector systems. Both the film and the image plate require x-ray exposure and then, be processed and read by some kind of digitizer or image reader. In this way, some level of spatial resolution and dynamic range will be lost. In situation when small peaks are of interest or accurate intensity function is required, these are not the desire techniques. Moreover, real-time experiments or experiments performed as a function of temperature will be extremely tedious and inefficient.

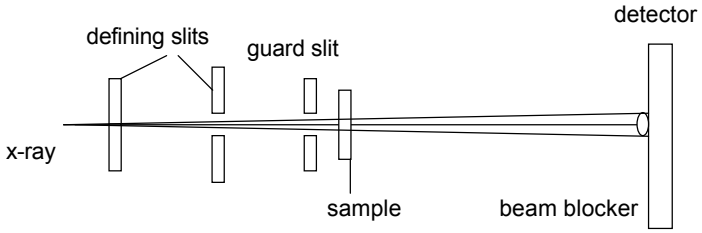


Figure 7: Optics for carrying out SAXS experiment using the 3-slit system

A basic requirement for a good experimental setup for SAXS is in the collimation. This is because SAXS is a measurement of extremely small intensity at very small angle, next to a very strong incident main beam. Hence, the scattering around the incident beam has to be as clean as possible and protected against parasitic scattering cause by the defining slits and beam blocker. Commonly used in the pin-hole technique for the in-house systems, is the 3 pin-hole slits system with different sizes, schematically shown in Figure 7. They have to be properly arranged and matched with the size of the beam blocker to obtain the clean primary beam and reach to the lowest angle. The 3$^{rd}$ slit is the guard slit which filters out the parasitic scattering from the defining slits. Not that the beam is diverging from the source. To avoid air scattering, the beam path has to be under vacuum, which inherently introduces 2 x-ray windows. The weak scattered x-ray from the sample has to penetrate these windows without changing the energy and the direction of the x-ray. The advantage of pin-hole technique is that anisotropic samples, for example fibers, films can be examined. By translating the sample, localize spot examination can also be carried out.

The more advanced 2-D gas proportional detector system has also been used. The heart of the detector is the multi-wire grid and the spatial resolution is limited to the wire spacings. Normally, this is limited to about 1 mm, even though some advances were made (0.2-0.3 mm) via the electronic and software developments. As a consequence, pin-hole SAXS instruments require long path lengths to expand the image for the detector to receive.

To increase the intensity, the 2$^{nd}$ method of using a line source is often used. The optics is

essentially similar to the pin-hole system shown in Figure 7. This method increases the flux of the incident beam, however only isotropic sample can be carried out. Unfortunately, because of the fix slit, desmearing of the data is needed. Again, there are 3 line slits properly arrange to minimized parasitic scattering are used. The adjustments on these slits are often very sensitive and difficult. So, Kratky block collimation as shown in Figure 8 was introduced and continued to being used today. It is easier to align and there are not too many adjustments. It can also achieve much smaller $k$ ($Å^{-1}$) value that the normal three slits system.

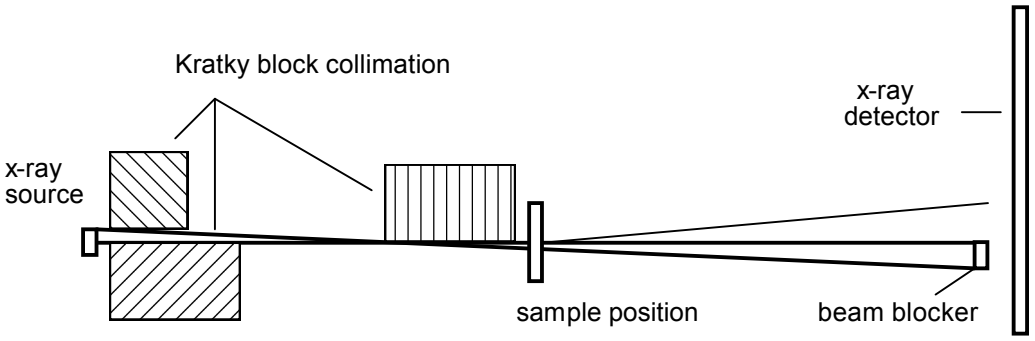


Figure 8: Kratky block collimation system

Another method of increasing the incident beam flux and improving the spatial resolution is by using focusing mirrors and monochromators. In order to achieve even smaller in *k,* Bonse-Hart technique is used. It was noted that by taking advantage of tighter energy filter, even smaller angle could be achieved. This is accomplished by having the x-ray bounce several times through a channel cut crystal on the incident end as well as the diffracted end. This technique also requires significant amount of alignments and are normally set up at dedicated beam line at the synchrotron sources. Again, this is also a line source and the issue of desmearing will have to be considered.

## XIII. Synchrotron Radiation

Undoubtedly, synchrotron radiation plays a major role in extending x-ray scattering capabilities. As pointed out in the introduction, unlike in-house x-ray source, synchrotron radiation has unique properties. The generation of synchrotron radiation will not be covered here. The x-rays generated by a synchrotron source is, highly collimated, highly polarized, tunable and high brightness. The probe size can be made small down to 2 μm, which essentially provided an in-sight into the composition of biological cell and local structure which are not possible using the in-house source.

The high collimation enables diffraction experiments to be carried out with improved precision. The peak width spread will be extremely small. The FWHM will be essentially due to the character of the sample and not the instrument. The divergence will be extremely small. By using an incident monochromator, unlike the in-house source, only mono-energetic beam is allowed to pass the incident monochromator. Because of the small divergence of the beam, SAXS experiment can be better setup.

To enhance the atomic speciation, anomalous WAXS and SAXS have also been developed and often used in an advanced laboratory. This arises from the tenability of the x-ray to the desired energies close to the absorption edges to enhance the scattering power by taking advantage of the anomalous scattering factors. These techniques will be covered in subsequent chapters of this volume by other authors. Clearly, there are more examples of utilizing the advantages of performing x-ray diffraction experiments using a synchrotron source.

## XIV. Concluding Remarks

In the field of materials characterization, x-ray scattering stands out to be the preferred method to obtain information on the structure and morphology of all sorts of materials. Essentially, x-ray is scattered by electrons and all matters have electrons. The domain size that fits both wide angle and small angle x-ray scattering ranges from a fraction of nm to 100 nm. At the low end, x-ray diffraction provided information on atomic positions, lattices, bond lengths, atomic speciation and structure. By carefully examining the character of the scattering, secondary information, like the crystallite size, lattice distortion and occupancy can also be extracted. Penetration depth of x-ray is also sufficiently high compare to x-ray photoemission or electron scattering, hence x-ray scattering can be considered as bulk probing.

With the theory and technique firmly understood, the method is used on more complex organic and polymeric systems. Unfortunately, in general these systems are not fully crystalline. They are semi-crystalline and more often, it is this semi-crystallinity that provided the unique properties of polymers. This semi-crystallinity in polymers essentially controls the morphology and this is probably one of the reasons for the development of small angle x-ray scattering.

Both the wide angle and small angle techniques are quite well developed. Basically, these characterization techniques are extended to different aspects of biological and lifescience. The structure of cells and cell tissues, lipid membranes, proteins and protein behavior, which are the building blocks of many organs in our anatomy are now being examined using the wide angle and small angle x-ray techniques.

The structures or nanostructure in biological and lifescience are generally very complex. However, with the advancement of computing power, high energy and spatial resolution of synchrotron source, these experiments on tissues, like cancer, tumors or sclerosis are now possible. Clearly, x-ray scattering, together with synchrotron and neutron scattering covers a whole range of characterization for organic and inorganic condensed matter, crystalline and semi-crystalline, amorphous structures. These experiences have also developed into the biological field and lifescience.

## XV. Acknowledgement

This work was performed under the auspices of the U.S. Department of Energy by University of California, Lawrence Livermore National Laboratory under Contract W-7405-Eng-48. Thanks to Dr. Art Nelson for reviewing the manuscript.

## XVI. References

The subject presented so far has been published in a number of fundamental books. Listed are some of the books used in writing this chapter.


1. Guinier, A., **X-ray Diffraction,** Freeman and Company, San Francisco, 1963.
2. Balta-Calleja F.J., and Vonk, C.G., **X-ray Scattering of Synthetic Polymers**, Elsevier, New York, 1989, Chapter 7.
3. Wang, J.I. and Harrison, I.R., **Methods of Experimental Physics: Volume 16: Polymers**, Ed. Fava, R.A., Academic Press, New York 1980.
4. Klug, H.P. and Alexander, L.E., **X-ray Diffraction Procedures**, John Wiley & Sons, New York, 1973
5. Alexander, L., **X-ray Diffraction Methods in Polymer Science**, Wiley-Interscience, New York, 1969.
6. Azaroff, L.V., **Elements of X-ray Crystallography**, McGraw-Hill Book Company, New York, 1968
7. Roe, R.J., **Methods of X-Ray and Neutron Scattering in Polymer Science**, Oxford University Press, New York, 1999.
8. Kostorz, G., **Treatise on Materials Science and Technology**, Academic Press Inc., New York 1979, 15, 227-286.
9. Richtmyer, F.K., Kennard, E.H. and Cooper, J.N., **Introduction to Modern Physics-6$^{th}$ Ed.**, McGraw-Hill, New York, 1969.
10. Warren, B.E., **X-ray Diffraction**, Addison-Wesley Publishing Co., Reading, MA, 1969.
11. Schwartz, L.H., Cohen, J.B., **Diffraction from Materials**, Springer-Verlar, New York, 1987.
12. Glatter, O. and Kratky, O., **Small Angle X-ray Scattering**, Academic Press, London 1982, 156.
13. Balta-Calleja, F.J. and Vonk, C.G., **X-ray Scattering of Synthetic Polymers**, Elsevier, New York, 1989, chapter 7.
14. Thomson, J.J., **Conduction of Electricity Through Gases**, 2$^{nd}$ ed., pg 321, and Compton, A.H. and Allison, S.K., **X-rays in Theory and Experiment**, 2$^{nd}$ ed. Van Nostrand-Reinhold, Princeton, NJ, 1935.
15. **International Table of Crystallography**, Vol. 1-4, by The International Union of Crystallography, ed. N.F.M. Henry and K. Lonsdale, The Kynoch Press, Birmingham, England, 1952.
16. Spruiell J.E. and Clark, E.S, **Methods of Experimental Physics, Chapter 6: X-ray Diffraction,** Fava, R.A. Editor, Academic Press, New York, 1980.
17. Bennett, C.H., **Serially deposited amorphous aggregates of hard spheres**, J. Appl. Phys. 1972, 43, 2727-2734, Boudreaux, D.S. and J.M. Gregor, J.M., **Structure simulation of transition-metal-metalloid glasses. III**, *J. Appl. Phys.*, 1977, 48 , 5057-5061.
18. Saw C.K. and Schwarz, R.B., **Chemical short-range order in dense random-packed models**, J. of the Less-Common Metals, 1988, 140, 385-393
19. Vaughan, D. (Ed), **X-ray data booklet**, Center for X-ray Optics, Lawrence Berkeley Laboratory, Berkeley, CA 1986 and Dyson, N.A., **X-rays in atomic and nuclear physics**, Longman, London, 1973, chapter 3.
20. Fernandez, M., Keyrilainen, J., Serimaa, R., Torkkeli, M., Karjalainen-Lindsberg, M-L.,

Tenhunen, M., Thomlinson, W., Urban, V. and Suortti, P., **Small-angle x-ray scattering studies of human breast tissue samples,** Phys. Med. Biol., 2002, 47, 577-592.
21. Lewis, R.A., Rogers, K.D., Hall, C.J., Towns-Andrews, E., Slawsom, S., Evans, A., Pinder, S.E., Ellis, I.O., Boggis, C.R.M., Hufton, A. and Dance, D.R., **Breast caner diagnosis using scattered x-rays,** J. Synchrotron Rad. 200, 7, 348-352, James, V, **Synchrotron fibre diffraction identifies and locates foetal collagenouos breast tissue associated with breast carcinoma,** J. Synchrotron Rad., 2002, 9, 71-76
22. Jaschouz, D., Paris, O., Roschger, P., Hwang, H.S., Fratzl, P., **Pole figure analysis of mineral nanoparticles orientation in individual trabecula of human vertebral bone,** J. Appl. Cryst. 2003, 36, 494-498.
23. Jager, I. and Fratzl, P., **Mineralized collagen fibrils: A mechanical model with a staggered arrangement of mineral particles,** Biophys. J., 2000, 79, 1737-1746
24. Laggner, P., **Physiochemical Methods in the Study of Biomembranes: Subcellular Biochemistry**, edited Hilderson H.J. and Ralston, G.B., Plenum Press, New York, 1994, 23, 11, 451-491.
25. Murray, C.B., Kagan, C.R. and Bawendi, M.G., **Synthesis and characterization of monodisperse nanocrystals and closed-packed nanocrystals assemblies**, Annu. Rev. Mater. Sci., 2000, 20, 545-610.
26. Stuhrmann, H.B. and Miller, A., **Small-angle scattering of biological structures**, J. Appl. Cryst. 1978, 11, 325-345.
27. Fratzl, P., **Cellulose and collagen: from fibres to tissues**, Current Opinion in Colloid and Interface Science, 2003, 8, 32-39.
28. Fratzl, P., Gupta, H.S., Paschalis, E.P., Roschger, P., **Structure and mechanical quality of the collagen-mineral nano-composite in bone**, J. Mater. Chem., 2004, 14, 2115-2123.
29. Abraham, T., Masakatsu, H. and Hirai, M., **Glycolipid based cubic nanoparticles: preparation and structural aspects,** Colloids and Surfaces B:Biointerfaces, 2004, 35, 107-117.